

Quantum-dot gain without inversion: Effects of dark plasmon-exciton hybridization

Dongxing Zhao,¹ Ying Gu,^{1,2,*} Jiarui Wu,¹ Junxiang Zhang,³ Tiancai Zhang,³ Brian D. Gerardot,⁴ and Qihuang Gong^{1,2}

¹State Key Laboratory for Mesoscopic Physics, Department of Physics, Peking University, Beijing 100871, China

²Collaborative Innovation Center of Quantum Matter, Beijing, China

³State Key Laboratory of Quantum Optics and Quantum Optics Devices, Institute of Opto-Electronics, Shanxi University, Taiyuan 030006, China

⁴Institute of Photonics and Quantum Sciences, SUPA, Heriot-Watt University, Edinburgh EH14 4AS, United Kingdom

(Received 19 November 2013; revised manuscript received 8 May 2014; published 20 June 2014)

We propose an initial-state-dependent quantum-dot gain without population inversion in the vicinity of a resonant metallic nanoparticle. The gain originates from the hybridization of a dark plasmon-exciton and is accompanied by efficient energy transfer from the nanoparticle to the quantum dot. This hybridization of the dark plasmon-exciton, attached to the hybridization of the bright plasmon-exciton, strengthens nonlinear light-quantum emitter interactions at the nanoscale, thus the spectral overlap between the dark and the bright plasmons enhances the gain effect. This hybrid system has potential applications in ultracompact tunable quantum devices.

DOI: 10.1103/PhysRevB.89.245433

PACS number(s): 78.67.Hc, 42.50.Gy, 73.20.Mf, 78.67.Bf

I. INTRODUCTION

With the development of nanotechnology, hybrid nanostructures from different photonic entities have attracted fundamental research interest, as they possess strong functionality that can far exceed that of the individual subunits [1,2]. For dispersive and absorptive plasmon nanostructures whose coupling coefficient generally lies between weak and strong coupling regimes, local field effects of surface plasmons enable plasmon-exciton hybridization in a closely packed quantum dot (QD)–metallic nanoparticle (MNP) system [3–13]. In the pioneering work by Zhang *et al.* [3], the plasmon-exciton interaction model included a feedback (i.e., self-interaction of the QD) setup. Several optical phenomena have been predicted from the hybrid mechanism, such as modified absorption spectra [3], tunable single-photon properties [4], enhanced Kerr nonlinearity [5,6], and controllable population and energy transfer [7,8]. Dark plasmons, which are nonradiative localized surface plasmon modes by virtue of having nonvanishing dipole moments [14], have more localized fields and store more energy than radiative bright modes [15,16]. Generally, dark plasmons cannot be excited by a plane wave [17,18]. In hybrid QD-MNP systems, without being attached to bright plasmon-exciton hybridization, dark plasmon-exciton hybridization cannot exist. Thus dark plasmon-exciton hybridization strengthens the nonlinear light-quantum emitter interaction and provides a novel means to tailor optical properties at the nanoscale.

Here, we propose a unique mechanism which utilizes the hybridization of a dark plasmon-exciton to induce QD gain. The interaction processes in this hybrid system (Fig. 1) can be described as follows. When incident light (I) resonantly couples to the system, it excites the dipole of transition $|2\rangle \leftrightarrow |3\rangle$ (μ_{23}^{QD}) and the bright plasmon of MNP (B^{MNP}) simultaneously. Since the QD and MNP are very close, generally 10–20 nm, μ_{23}^{QD} will excite B^{MNP} and dark plasmons (D^{MNP}) due to the overlap of the spectral width between the bright plasmon and dark plasmons. Then these excited modes

B^{MNP} and D^{MNP} will retroact on the QD. In other words, besides $I \rightarrow \mu_{23}^{\text{QD}}$, there are two other pathways to act on the QD: $I \rightarrow B^{\text{MNP}} \rightarrow \mu_{23}^{\text{QD}}$ and $\mu_{23}^{\text{QD}} \rightarrow B^{\text{MNP}} + D^{\text{MNP}} \rightarrow \mu_{23}^{\text{QD}}$, which implies that without the excitation of bright plasmons or the QD exciton, the dark plasmons cannot be directly excited. The strong retroaction of these dark plasmons on the QD leads to the gain without population inversion in the QD.

Gain without inversion (GWI) originating from quantum coherence effects was first proposed in coherent atomic ensembles [19–21]. Recently, GWI was experimentally realized in single nanostructures including a quantum well [22] and a QD [23]. Here, using hybridization of a dark plasmon-exciton, an initial-state-dependent GWI effect in the hybrid three-level QD-MNP system is demonstrated. It is, in principle, different from previous work in that, through the self-interaction of the QD, the dark plasmons resonantly transfer the energy from the MNP to the QD to form gain without population inversion. The extent of the spectral overlap between dark and bright plasmons determines the magnitude of gain, while higher order dark plasmons lead to a larger gain regime. Such hybrid QD-MNP systems may find applications in ultracompact active quantum devices.

The paper is organized as follows. In Sec. II we present the theoretical model of the hybrid system, which includes the feedback of dark plasmons of the MNP. We solve this model both in the steady state and dynamically. The phenomenon of QD GWI and its features are presented in Sec. III. We analyze the physical mechanism in Sec. IV and find that the hybridization of dark plasmons and the exciton plays a vital role. In Sec. V we discuss the feasibility of experimental realization of the proposed mechanism. Finally, we present our conclusions in Sec. VI.

II. INTERACTION MODEL WITH DARK-PLASMON FEEDBACK

We consider a hybrid system composed of a Λ -type three-level QD and a metallic nanosphere with radius a , separated by distance R , embedded in a dielectric host with dielectric constant ϵ_b , as shown in Fig. 1. In ladder and V-type

*ygu@pku.edu.cn

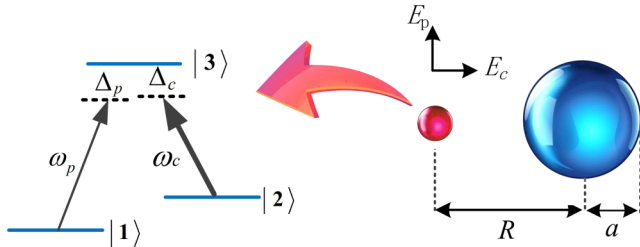


FIG. 1. (Color online) Schematic of a hybrid system composed of a Λ -type three-level QD and a metallic nanosphere.

QD-MNP hybrid systems, plasmon-induced transparency [24] and a shift of the transparency windows [25] in the absorption spectra of MNPs have been predicted. In our system, only one transition, $|2\rangle \leftrightarrow |3\rangle$, is on-resonance with the MNP surface plasmons, and the other transition, $|1\rangle \leftrightarrow |3\rangle$, is off-resonance. The system is driven by a weak probe field, $E_p \cos(\omega_p t)$, coupling to $|1\rangle$ and $|3\rangle$ and a strong control field, $E_c \cos(\omega_c t)$, exciting both the transition $|2\rangle \leftrightarrow |3\rangle$ and the surface plasmon resonance of the MNP. It is assumed that the dimensions of the system are significantly smaller than the wavelength of incident light, so we can use the quasistatic approximation and ignore retardation effects in the system. The positive-frequency component of the electric field felt by the transition $|2\rangle \leftrightarrow |3\rangle$ can be divided into three parts: $E_{23}^+ = (E_1^+ + E_2^+ + E_3^+ \rho_{32})e^{-i\omega_c t}$, where $E_1^+ = \frac{E_c}{2}$; $E_2^+ = \frac{a^3 E_c}{R^3} \alpha_1(\omega_c)$, with $\alpha_1(\omega_c) = [\varepsilon_m(\omega_c) - \varepsilon_b] / [\varepsilon_m(\omega_c) + 2\varepsilon_b]$ and ε_m being the dielectric constant of the MNP, which comes from the polarization field of the MNP induced by the control field; and $E_3^+ \rho_{32} = \sum_{n=1}^{\infty} \frac{(n+1)^2 a^{2n+1} \mu_{23} \rho_{32}}{4\pi \varepsilon_0 \varepsilon_b R^{2n+4}} \alpha_n(\omega_c)$, with $\alpha_n(\omega_c) = \frac{\varepsilon_m(\omega_c) - \varepsilon_b}{\varepsilon_m(\omega_c) + \frac{n+1}{n} \varepsilon_b}$ and dipole moment μ_{23} , which describes the feedback that the QD received from the MNP. Multipole effects of the MNP have been shown to cause spectral shifts and modification of the Fano line shape [11,12]. But for the parameters used in this work, the effects of modes of $n > 1$ belong to dark plasmon-exciton hybridization from the spectral overlap between bright and dark plasmons.

In the dipole and rotating-wave approximations, the Hamiltonian of the hybrid system in the interaction picture has the form

$$H = \hbar(\Delta_p - \Delta_c)\sigma_{22} + \hbar\Delta_p\sigma_{33} - \hbar[(\Omega'_c + G_c\rho_{32})\sigma_{32} + \text{H.c.}] - \hbar(\Omega_p\sigma_{31} + \text{H.c.}), \quad (1)$$

where $\Omega'_c = \Omega_c + \frac{\mu_{23}E_3^+}{\hbar}$ and $G_c = \frac{\mu_{23}E_3^+}{\hbar}$, with drive and probe Rabi frequencies $\Omega_c = \frac{\mu_{23}E_1^+}{\hbar}$ and $\Omega_p = \frac{\mu_{13}E_p}{2\hbar}$; $\Delta_c = \omega_3 - \omega_2 - \omega_c$ and $\Delta_p = \omega_3 - \omega_1 - \omega_p$ are the control and probe light detuning, $\sigma_{ij} = |i\rangle\langle j|$. Then the dynamics of the system are governed by the master equation:

$$\begin{aligned} \dot{\rho}_{11} &= -i\Omega_p\rho_{13} + i\Omega_p^*\rho_{31} + \Gamma_{31}\rho_{33}, \\ \dot{\rho}_{22} &= -i(\Omega_c + G_c\rho_{32})\rho_{23} + i(\Omega_c^* + G_c^*\rho_{23})\rho_{32} + \Gamma_{32}\rho_{33}, \\ \dot{\rho}_{31} &= -i\Delta_p\rho_{31} + i(\Omega_c + G_c\rho_{32})\rho_{21} - i\Omega_p(\rho_{33} - \rho_{11}) \\ &\quad - \frac{1}{2}\gamma_{31}\rho_{31}, \end{aligned}$$

$$\begin{aligned} \dot{\rho}_{32} &= -i\Delta_c\rho_{32} + i\Omega_p\rho_{12} - i(\Omega_c + G_c\rho_{32})(\rho_{33} - \rho_{22}) \\ &\quad - \frac{1}{2}\gamma_{32}\rho_{32}, \\ \dot{\rho}_{21} &= -i(\Delta_p - \Delta_c)\rho_{21} - i\Omega_p\rho_{23} + i(\Omega_c^* + G_c^*\rho_{23})\rho_{31} \\ &\quad - \frac{1}{2}\gamma_{21}\rho_{21}, \end{aligned} \quad (2)$$

with $\rho_{11} + \rho_{22} + \rho_{33} = 1$, $\rho_{ij} = \rho_{ji}^*$. Here Γ_{31} and Γ_{32} describe the spontaneous decay rates from state $|3\rangle$ to states $|1\rangle$ and $|2\rangle$. We also introduce energy-conserving dephasing rates γ_{3d} and γ_{2d} of states $|3\rangle$ and $|2\rangle$. For convenience, we define coherence decay rates as $\gamma_{31} = \Gamma_{31} + \Gamma_{32} + \gamma_{3d}$, $\gamma_{32} = \gamma_{31} + \gamma_{2d}$, and $\gamma_{21} = \gamma_{2d}$. This set of equations resembles the dynamics of the EIT system in the $R \rightarrow \infty$ limit [26]. In the following, we solve these equations both in the steady state and dynamically.

We note that the self-interaction term $G_c\rho_{32}$ in the Hamiltonian, which is a result of plasmon-exciton hybridization, leads to nonlinear elements in the set of equations of ρ , which may cause the coexistence of multisolutions. In this regime of a hybrid two-level QD-MNP system, the strong and nonlinear self-interaction of a QD leads to several interaction regions where the double-peaked Fano structure, bistability, and discontinuities in the absorption spectra can occur [9,10]. Here, we find that there are at most three solutions for certain parameters. The first solution is the general EIT solution, where most of the population is trapped in state $|1\rangle$ due to the near-field action on the QD, thus ρ_{32} is extremely small and the effect of self-interaction becomes negligible. The second solution is unstable; that is, even though the initial state is very close to this solution, the final state still evolves to the first or third solution. The third solution appears when the self-interaction term $G_c\rho_{32}$ is large and strong nonlinear interaction leads to gain of the applied field in the transition $|2\rangle \leftrightarrow |3\rangle$, shown as the upper (red) curve in Fig. 2(a). The evolutions of the three solutions are described in the Appendix.

III. QUANTUM-DOT GAIN WITHOUT INVERSION

Figure 2 displays the typical GWI phenomenon in the hybrid system. Here, the gain of applied light on the transition $|2\rangle \leftrightarrow |3\rangle$ is expressed as the imaginary part of $-2\hbar\omega_c\Omega_c\rho_{32}$ and the absorption of MNP is $2\varepsilon_0\omega_c\text{Im}[\varepsilon_m(\omega_c)] \int \langle E_{\text{MNP}}^+ E_{\text{MNP}}^- \rangle dV$, with $\langle \dots \rangle$ denoting the average over time and E_{MNP}^+ (E_{MNP}^-) being the positive (negative)-frequency component of the electrical field inside the MNP [3,11]. The dielectric constant of silver nanoparticles $\varepsilon_m(\omega)$ is taken from experimental data [27] and $\varepsilon_b = 1$. For the QD, we take the resonant energy between $|2\rangle$ and $|3\rangle$ to be 3.47 eV, which is within the plasmon peak of a silver MNP in vacuum (3.5 eV) [28]. Other parameters are set as follows: $\Gamma_{31} = \Gamma_{32} = 2 \times 10^9 \text{ s}^{-1} \equiv \Gamma$, $\gamma_{2d} = 0.001\Gamma$ and $\gamma_{3d} = 0$, and $\mu_{23} = 0.5 \text{ enm}$. When scanning the probe light, gain of the coupling light appears upon the transition $|2\rangle \leftrightarrow |3\rangle$ [see upper (red) curve in Fig. 2(a)], which originates from a strong nonlinear interaction between the QD and the MNP. In the high-gain regime there is a large decrease in the absorption spectrum of the MNP [lower (red) curve in Fig. 2(b)] compared to the energy absorption without the QD [dotted (green) curve],

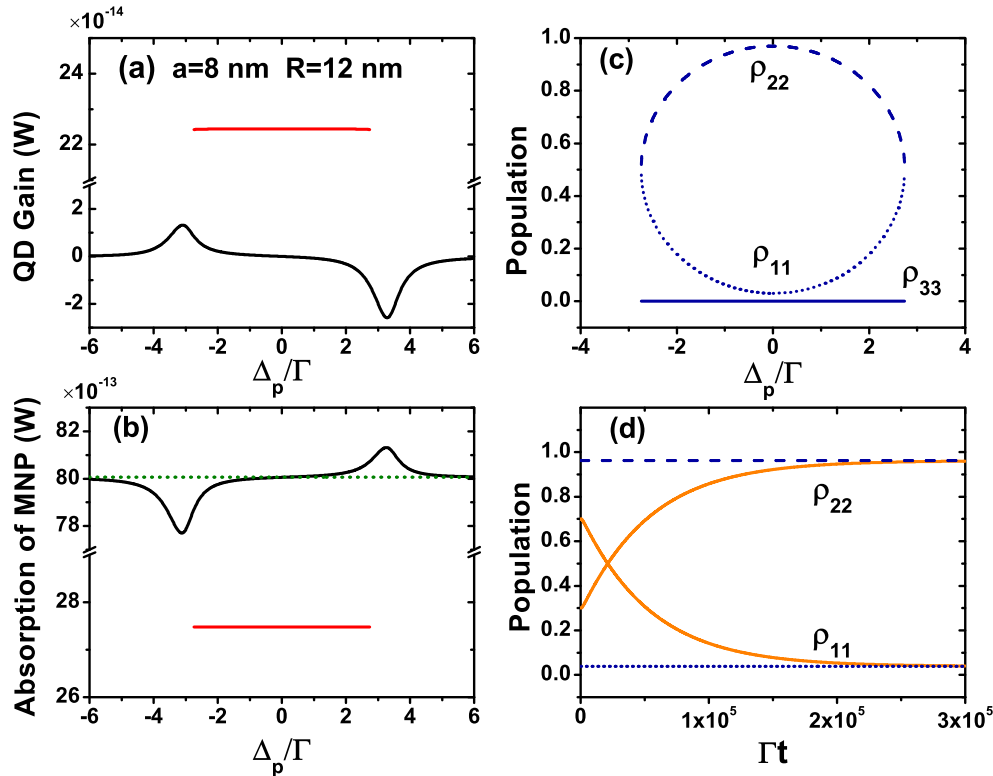


FIG. 2. (Color online) Gain without population inversion. (a) QD gain in the transition $|2\rangle \leftrightarrow |3\rangle$ and (b) energy absorption in the MNP for trivial EIT (black curve) and GWI [horizontal (red) line] solutions. The dotted (green) curve is the energy absorption in the MNP without the QD. (c) QD population for the GWI solution. $\rho_{22} > \rho_{11} \gg \rho_{33}$. (d) QD population dynamics. The initial state is set to be $|\psi(0)\rangle = \sqrt{\frac{7}{10}}|1\rangle + \sqrt{\frac{3}{10}}|2\rangle$. Dashed and dotted curves show the steady population of the GWI solution. System parameters: $a = 8$ nm, $R = 12$ nm, $\Omega_p = 0.005\Gamma$, $\Omega_c = 0.5\Gamma$, $\Delta_c = 0$, and $\Delta_p = -0.5$ [only for (d)].

signifying an efficient energy transfer from the MNP to the QD. The population distributions in the gain regime are shown in Fig. 2(c), where the gain without population inversion occurs; i.e., $\rho_{22} > \rho_{11} \gg \rho_{33}$. In fact, there is almost no population in state $|3\rangle$. At $\Delta_p/\Gamma = 3.3$, there also exists a gain in the trivial solution (black curve) where there is no population inversion, in agreement with the previously reported gain results [8].

Unlike previously reported GWI in atomic and pure QD systems [19–23], GWI in the hybrid QD-MNP system comes from the third solution of nonlinear equations $\dot{\rho}$, thus it is initial state dependent. This means that, through a deterministically prepared QD initial state, whether or not gain appears can be controlled. The strongly tunable gain could be exploited for ultracompact QD lasers or quantum logic gates. Figure 2(d) displays the evolution of ρ_{11} and ρ_{22} as a function of time Γt . It is shown that even when state $|1\rangle$ is initially populated at 70%, the system evolves to $\rho_{22} > \rho_{11}$ in the solution of GWI. Further details about the dependence of the GWI on the initial state can be found in the Appendix.

IV. EFFECTS OF DARK PLASMON-EXCITON HYBRIDIZATION

In order to explore the underlying mechanism responsible for the retroaction of the dark plasmons on the QD which leads to GWI, the energy absorption of the MNP excited by a nearby dipole and the corresponding gain are plotted in Fig. 3. The

nearby dipole resembles the dipole μ_{23} ($\rho_{23} + \rho_{32}$) of the QD. As shown in Fig. 3(a), this dipole excites not only the bright plasmon, but also the dark plasmons, both of which feedback on the QD. The extent of the overlap between the bright plasmon and the dark plasmons determines the magnitude and extent of the gain regime [Figs. 3(b)–3(d)]. At $\omega_{32} = 3.53$ eV, the overlap reaches the maximum, leading to a gain magnitude more than twice that at $\omega_{32} = 3.47$ eV [marked by the magenta points in Fig. 3(b)].

To understand further how the hybridization of the dark plasmon-exciton contributes to the GWI, we investigate the gain by considering one bright plasmon only ($N = 1$), one bright and one dark plasmon ($N = 2$), and so on. As shown in Figs. 3(c) and 3(d), when $N = 1$, i.e., only the retroaction of the dipole mode on the QD is considered, the gain is negative (signifying absorption). Gain starts to appear only when we take the effect of dark plasmons into account. $N = 10$ means that we consider the sum of 10 orders of plasmons (almost approaching the limit of $N \rightarrow \infty$). For the frequency $\omega_{32} = 3.47$ eV, as N increases both the gain and the range of the gain regime increase and when $N \rightarrow \infty$ they reach the maximum [Fig. 3(c)]. However, for $\omega_{32} = 3.53$ eV in Fig. 3(d), with increasing N there is eventually a fall after the initial rise in the gain, leading to the observation that higher order plasmons do not necessarily correspond to a larger gain.

The population distribution for the GWI solution can be understood in the following way. Assume that $\rho_{33} \approx 0$ and

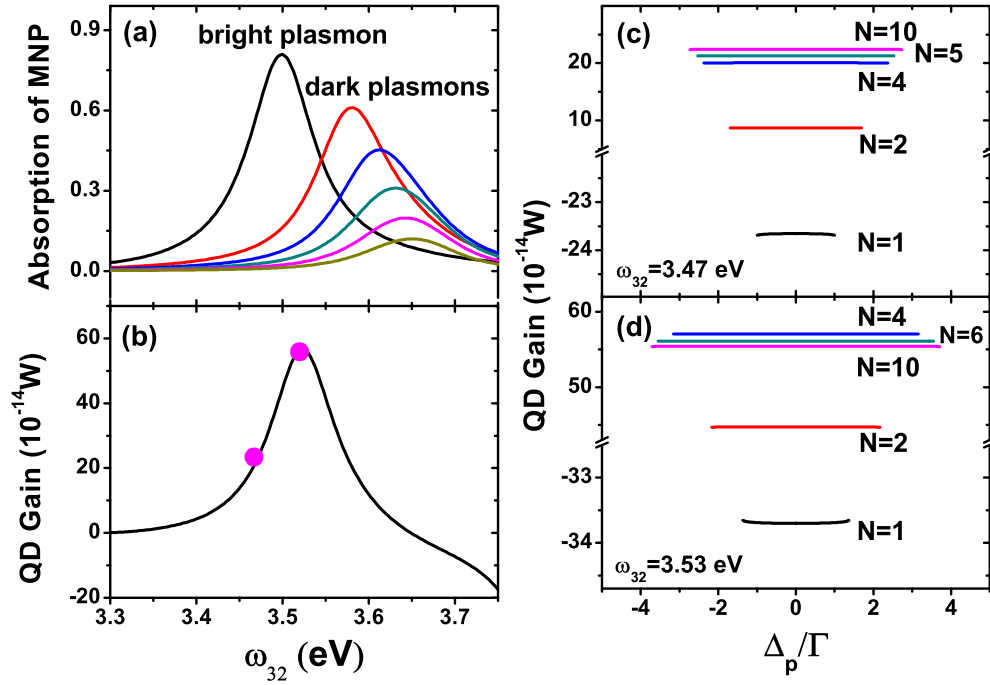


FIG. 3. (Color online) Mechanism of using the retroaction of dark plasmons to produce the GWI. (a) Energy absorption of MNP contributed by a bright plasmon (dipole mode) and dark plasmons (quadruple mode, octuple mode, etc.), which are excited by a nearby dipole. (b) QD gain as a function of the overlap of bright and dark plasmons. QD gain for (c) $\omega_{32} = 3.47$ eV and (d) $\omega_{32} = 3.53$ eV obtained by considering the bright mode only ($N = 1$), both dipole and quadruple modes ($N = 2$), and higher order modes ($N = 4, 5, 6, 10$). Other parameters are the same as in Fig. 2, except that $\Delta_p = 0.001$ and $\Delta_c = 0$.

$\rho_{21} \approx 0$; we obtain that $G_c \rho_{32} \approx -\Omega'_c$, which means that the self-interaction $G_c \rho_{32}$ has a π phase shift relative to the Ω'_c , thus these two parts interfere destructively and cancel each other to some degree. Finally, the net field felt by the transition $|2\rangle \leftrightarrow |3\rangle$ is far less than the field in transition $|1\rangle \leftrightarrow |3\rangle$, which explains why the population in level $|1\rangle$ is less than that in level $|2\rangle$.

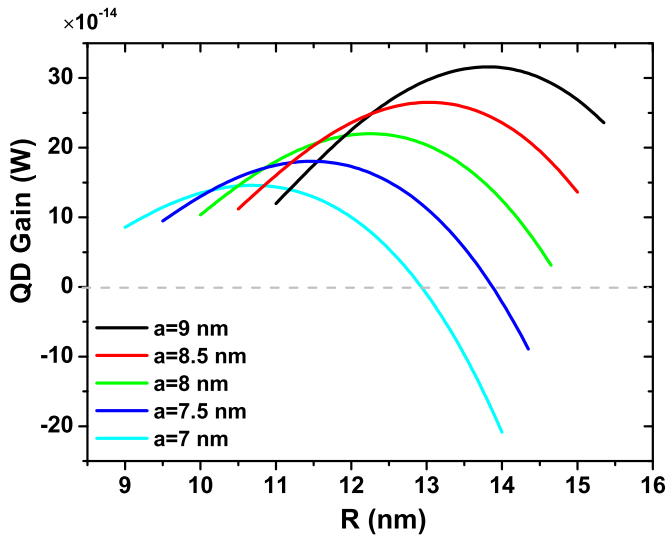


FIG. 4. (Color online) Optimal distances of GWI for different-sized MNPs. Other parameters are the same as in Fig. 2 except that $\Delta_p = 0.001$.

Subsequently, we found that with varying distance R (for fixed MNP radius a), there is a maximum in the gain curve, signifying the optimal distance for the GWI (see Fig. 4). It is also found that increasing a increases the optimal R , e.g., when a is increased from 7 to 9 nm the optimal R increases from 10.5 to 14 nm. Additionally, increasing R leads to increased gain due to the hybridization of higher order dark plasmons with the exciton, which can contribute to gain effects.

The gain of the control light can be obtained only when the probe detuning enters the gain regime. This allows us to turn on or off the gain effect using the probe field. The gain regime can be modulated effectively. It is found that, when Ω_p is extremely small, the gain regime is not separately relevant to the values of Ω_c and Ω_p , but to the ratio between them. The gain regime broadens when the ratio Ω_c/Ω_p is decreased (Table I). For the same distance, the larger MNP with higher order dark plasmons generally has a wider gain regime (Table II). As R increases, the gain regime narrows and, finally, vanishes because the coupling between the QD and plasmons of the MNP becomes weak.

TABLE I. The gain regime Δ_p/Γ of the QD for different Ω_c/Ω_p and R values. Other parameters are the same as in Fig. 2. The 0 denotes that no gain regime was found.

Ω_c/Ω_p	$R = 12$ nm	$R = 13$ nm	$R = 14$ nm	$R = 15$ nm
100	(-2.74, 2.74)	(-1.57, 1.57)	(-0.80, 0.80)	0
75	(-3.76, 3.76)	(-2.27, 2.27)	(-1.39, 1.39)	(-0.72, 0.72)
70	(-5.75, 5.75)	(-3.59, 3.59)	(-2.36, 2.36)	(-1.56, 1.56)

TABLE II. The gain regime Δ_p/Γ of the QD for different a and R values. Other parameters are the same as in Fig. 2. A 0 indicates that no gain regime was found.

a (nm)	$R = 12$ nm	$R = 13$ nm	$R = 14$ nm	$R = 15$ nm
7	(-1.87, 1.87)	(-1.04, 1.04)	(-0.24, 0.24)	0
8	(-2.74, 2.74)	(-1.57, 1.57)	(-0.80, 0.80)	0
9	(-4.60, 4.60)	(-2.39, 2.39)	(-1.32, 1.32)	(-0.56, 0.56)

V. DISCUSSION OF EXPERIMENTAL FEASIBILITY

We now discuss the experimental feasibility of the hybrid system. First, three-level Λ systems can be realized in self-assembled InGaAs QDs charged with a single spin under an external applied in-plane magnetic field (Voigt geometry) [29]. In this scenario, Zeeman split single-spin states form the two ground states of the Λ system, each of which is dipole coupled with orthogonal linear polarizations to a common excited trion state. Coherent population trapping has been achieved with single-hole spins in single QDs [30,31] and electron spins in single [32] or coupled QDs [33]. In these InGaAs QDs, $\omega_{32} \sim 1.3$ eV and $\omega_{21} \sim 0.1$ meV. To match the specific Λ system considered in this report, ω_{32} could be increased to ~ 3.5 eV using a different materials system (e.g., GaN QDs [34]) and ω_{21} could be increased significantly by working with larger magnetic fields and engineering larger g factors (e.g., with QD molecules [35]). Here the QD is treated as point-like and its mesoscopic character is neglected, for simplicity. After taking the mesoscopic size of QD into account, the interaction between QD and MNP can be enhanced through appropriate arrangement [36]. The shortcoming may be that because of the fast spatial decay of the near field of plasmon, it is difficult to locate the QD very close to the MNP surface, which would inevitably lead to degradation of the QD quantum efficiency and dephasing [36,37]. Though we have used the QD during our calculation, the mechanism proposed in our paper is not restricted to the QD only. Other alternative three-level Λ systems with a large dipole moment, such as single organic molecules [38], may be considered.

Then the MNP and QD coated with DNA molecules can self-assemble [39] into individual QD-DNA-MNP complexes [40] and hybrid planet-satellite nanoclusters [41]. The distance between the QD and the MNP is tunable by using different numbers of DNA bases [40,41]. In addition, one can use scanning tunneling microscopes and atomic force microscopes to manipulate and assemble different components at the nanometer scale [1]. Quenching of QD fluorescence [40] and second harmonic generation [42] in hybrid the QD-MNP system have been experimentally investigated. Finally, the measurements of the hybrid system could be made either with a simple confocal microscope or based on nanofiber-based optical sensors [43,44].

VI. CONCLUSIONS

In summary, we have found the QD gain without population inversion induced by the hybridization of a dark plasmon-exciton in a hybrid three-level QD-MNP system. The gain mechanism is unique to previously reported GWI; it

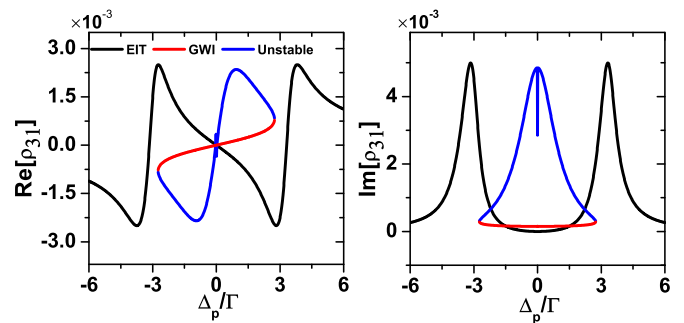


FIG. 5. (Color online) Real (left) and imaginary (right) part of ρ_{31} . Three steady solutions appear for the parameters $a = 8$ nm, $R = 12$ nm, $\Omega_p = 0.005\Gamma$, $\Omega_c = 0.5\Gamma$, $\omega_{32} = 3.47$ eV, and $\Delta_c = 0.0$.

originates from the retroaction of dark plasmons, expressed as an efficient energy transfer from the MNP to the QD. We have also discussed how this hybridization, in various parameters, affects the extent and magnitude of the gain regime. Dark plasmon-exciton hybridization in the hybrid QD-MNP system will have far-reaching effects in the generation of single photons and nonlinear optical properties. Moreover, the ultrasmall structures and excellent controllability of the hybrid system provide opportunities for applications in ultracompact QD lasers, quantum logic operations, solar cells, and light-emitting materials with plasmonic nanostructures. Finally, this investigation of moderate coupling in dispersive and absorptive plasmon nanostructures fills the gap of quantum optical properties lying between strong and weak coupling.

ACKNOWLEDGMENTS

Y.G. thanks F. J. Garcia-Vidal for useful discussions. This work was supported by the National Key Basic Research Program under Grant No. 2013CB328700, the National Natural Science Foundation of China under Grant Nos. 91121018, 11374025, 91221304, and 11121091, the NFFTS under Grant Nos. J1030310 and J1103205, the Royal Society, EPSRC, and the ERC.

APPENDIX: DYNAMICS OF THREE SOLUTIONS AND INITIAL-STATE DEPENDENCE

In this Appendix, through the dynamical processes, we present a detailed verification of the stability of multisolutions. The nonlinear items in the master equation contributed by the self-interaction are the mathematical origin of the multi-

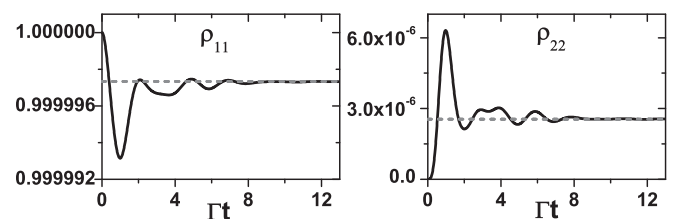


FIG. 6. Population dynamics of the EIT solution. The QD would evolve to the EIT solution if the initial state were $|\psi(0)\rangle = |1\rangle$. $\Delta_p = -0.5\Gamma$; other parameters are the same as in Fig. 5.

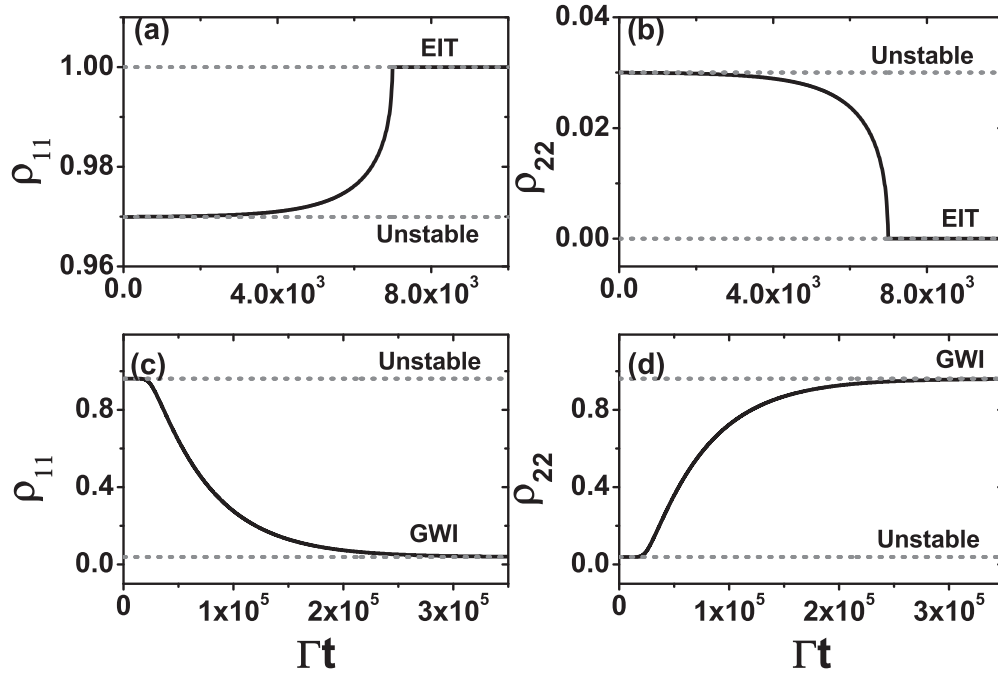


FIG. 7. Instability of the second solution. The $\rho(\infty)$ is either the EIT (a, b) or the GWI (c, d) solution according to different initial states $\rho(0)$ (very close to the second solution). Dashed lines show the steady-state population distribution for three solutions. Parameters are the same as in Fig. 6.

solutions. There exists only one solution when the coupling between the QD and the MNP is weak. However, when the distance between the QD and the MNP is decreasing, the self-interaction is enhanced and multisolutions appear. In the steady state, there are three solutions at most, which is in agreement with the situation of the hybrid two-level QD-MNP

system [9,10]. However, by the dynamical evolution from different initial states, it is verified that the first (EIT) and third (GWI) solutions are stable, while the second solution is unstable.

To illustrate the multisolution property of this hybrid system, the real and imaginary parts of ρ_{31} as a function of the

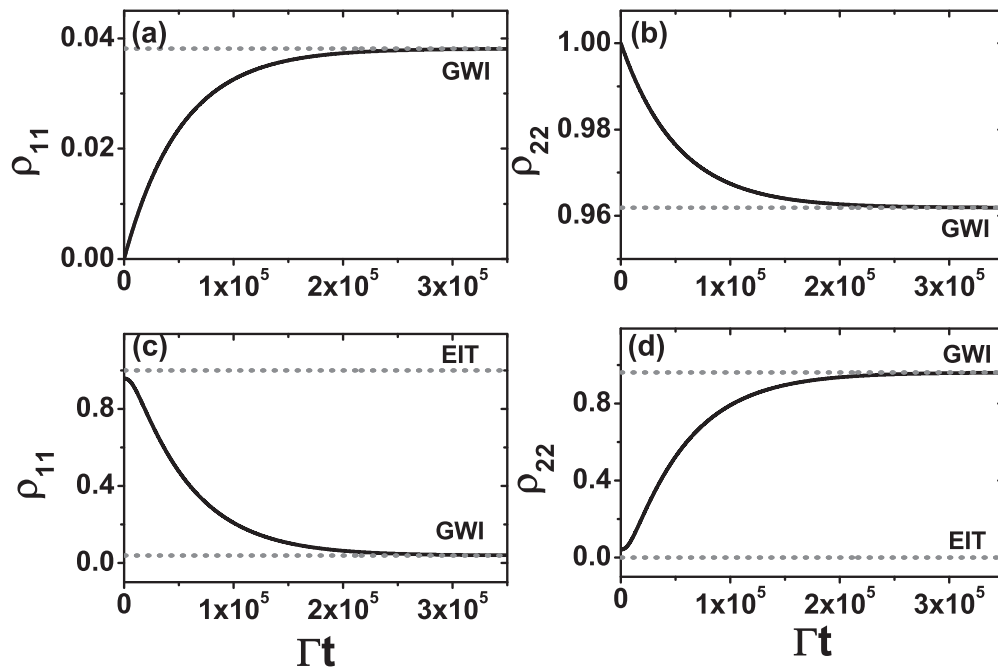


FIG. 8. Population dynamics of the GWI solution. The QD would evolve to the GWI solution if the initial state were $|\psi(0)\rangle = |2\rangle$ [for (a) and (b)] or a mixed state $\rho_{11}(0) = 0.96, \rho_{22}(0) = 0.04$ [for (c) and (d)]. Dashed lines show the steady-state population distributions for GWI and EIT solutions. Parameters are the same as in Fig. 6.

probe detuning Δ_p/Γ are shown in Fig. 5. In addition to the trivial EIT solution (black curve), there exist two new solutions (blue and red curves). The first is the EIT solution, which is characterized by $\rho_{11} \gg \rho_{22}$. In this case, the self-interaction is very weak, thus the majority of the populations is in level $|1\rangle$; i.e., ρ_{32} is near 0. The impact of the MNP on the QD is only the near field of the bright plasmon excited by the incident control field. The splitting of sidebands in the EIT window increases as the distance R decreases due to the weak QD-plasmon interaction [45]. This steady solution can be obtained under the condition that the initial state of the QD $|\psi(0)\rangle = |1\rangle$ (See Fig. 6).

The second solution shows a similar property of the population distribution ($\rho_{11} > \rho_{22}$) to the EIT solution. However, it is hard to find an initial state which will evolve to this solution. Even if we set the initial state to be very close to this solution, the state will evolve to other solutions. As shown in Fig. 7,

we introduced two different minor deviations to the second solution and then set them to be the initial state, but finally, $\rho(\infty)$ is either the EIT or the GWI solution. Thus we can conclude that the second solution is unstable and we have discarded it in the physical discussions.

There are more populations in state $|2\rangle$ than in state $|1\rangle$ for the GWI solution. In this case, the feedback $\rho_{32}G_c$ of dark plasmons is large, which leads to an energy transfer from the MNP to the QD. After the dynamical evolution of the GWI solution is performed, we found that it has the advantage of easy accessibility. If the initial state is set to be $|\psi(0)\rangle = |2\rangle$, the QD will evolve to the GWI solution [Figs. 8(a) and 8(b)]. However, as shown in Figs. 8(c) and 8(d), this GWI solution can be obtained even if there are more populations in state $|1\rangle$ (96% of populations are in state $|1\rangle$ for this case) than in state $|2\rangle$ at $t = 0$. This effect may provide a platform for quantum state preparation and population transfer [7,46,47].

[1] O. Benson, *Nature* **480**, 193 (2011).
 [2] M. S. Tame, K. R. McEnery, S. K. Ozdemir, J. Lee, S. A. Maier, and M. S. Kim, *Nat. Phys.* **9**, 329 (2013).
 [3] W. Zhang, A. O. Govorov, and G. W. Bryant, *Phys. Rev. Lett.* **97**, 146804 (2006).
 [4] A. Ridolfo, O. Di Stefano, N. Fina, R. Saija, and S. Savasta, *Phys. Rev. Lett.* **105**, 263601 (2010).
 [5] J.-B. Li, N.-C. Kim, M.-T. Cheng, L. Zhou, Z.-H. Hao, and Q.-Q. Wang, *Opt. Express* **20**, 1856 (2012).
 [6] Z. Lu and K.-D. Zhu, *J. Phys. B* **41**, 185503 (2008).
 [7] E. Paspalakis, S. Evangelou, and A. F. Terzis, *Phys. Rev. B* **87**, 235302 (2013).
 [8] S. G. Kosionis, A. F. Terzis, S. M. Sadeghi, and E. Paspalakis, *J. Phys.: Condens. Matter* **25**, 045304 (2013).
 [9] R. D. Artuso and G. W. Bryant, *Nano Lett.* **8**, 2106 (2008).
 [10] R. D. Artuso and G. W. Bryant, *Phys. Rev. B* **82**, 195419 (2010).
 [11] J.-Y. Yan, W. Zhang, S. Duan, X.-G. Zhao, and A. O. Govorov, *Phys. Rev. B* **77**, 165301 (2008).
 [12] R. D. Artuso, G. W. Bryant, A. Garcia-Etxarri, and J. Aizpurua, *Phys. Rev. B* **83**, 235406 (2011).
 [13] M. R. Singh, *Nanotechnology* **24**, 125701 (2013).
 [14] M. Liu, T.-W. Lee, S. K. Gray, P. Guyot-Sionnest, and M. Pelton, *Phys. Rev. Lett.* **102**, 107401 (2009).
 [15] D. Solis, B. Willingham, S. L. Nauert, L. S. Slaughter, J. Olson, P. Swanglap, A. Paul, W.-S. Chang, and S. Link, *Nano Lett.* **12**, 1349 (2012).
 [16] V. Giannini, G. Vecchi, and J. Gómez Rivas, *Phys. Rev. Lett.* **105**, 266801 (2010).
 [17] J. A. Fan, C. Wu, K. Bao, J. Bao, R. Bardhan, N. J. Halas, V. N. Manoharan, P. Nordlander, G. Shvets, and F. Capasso, *Science* **328**, 1135 (2010).
 [18] J. A. Fan, K. Bao, C. Wu, J. Bao, R. Bardhan, N. J. Halas, V. N. Manoharan, G. Shvets, P. Nordlander, and F. Capasso, *Nano Lett.* **10**, 4680 (2010).
 [19] S. E. Harris, *Phys. Rev. Lett.* **62**, 1033 (1989).
 [20] M. O. Scully, S.-Y. Zhu, and A. Gavrielides, *Phys. Rev. Lett.* **62**, 2813 (1989).
 [21] W. E. van der Veer, R. J. J. van Diest, A. Dönszelmann, and H. B. van Linden van den Heuvell, *Phys. Rev. Lett.* **70**, 3243 (1993).
 [22] M. D. Frogley, J. F. Dynes, M. Beck, J. Faist, and C. C. Phillips, *Nat. Mater.* **5**, 175 (2006).
 [23] X. Xu, B. Sun, P. R. Berman, D. G. Steel, A. S. Bracker, D. Gammon, and L. J. Sham, *Science* **317**, 929 (2007).
 [24] S. M. Sadeghi, L. Deng, X. Li, and W.-P. Huang, *Nanotechnology* **20**, 365401 (2009).
 [25] M. R. Singh, D. G. Schindel, and A. Hafez, *Appl. Phys. Lett.* **99**, 181106 (2011).
 [26] M. Fleischhauer, A. Imamoglu, and J. P. Marangos, *Rev. Mod. Phys.* **77**, 633 (2005).
 [27] P. B. Johnson and R. W. Christy, *Phys. Rev. B* **6**, 4370 (1972).
 [28] C. F. Bohren and D. R. Huffman, in *Absorption and Scattering Light by Small Particles* (Wiley, New York, 1983).
 [29] X. Xu, Y. Wu, B. Sun, Q. Huang, J. Cheng, D. G. Steel, A. S. Bracker, D. Gammon, C. Emary, and L. J. Sham, *Phys. Rev. Lett.* **99**, 097401 (2007).
 [30] D. Brunner, B. D. Gerardot, P. A. Dalgarno, G. Wüst, K. Karrai, N. G. Stoltz, P. M. Petroff, and R. J. Warburton, *Science* **325**, 70 (2009).
 [31] J. Houel, J. H. Prechtel, A. V. Kuhlmann, D. Brunner, C. E. Kuklewicz, B. D. Gerardot, N. G. Stoltz, P. M. Petroff, and R. J. Warburton, *Phys. Rev. Lett.* **112**, 107401 (2014).
 [32] X. Xu, B. Sun, P. R. Berman, D. G. Steel, A. S. Bracker, D. Gammon, and L. J. Sham, *Nat. Phys.* **4**, 692 (2008).
 [33] K. M. Weiss, J. M. Elzerman, Y. L. Delley, J. Miguel-Sanchez, and A. Imamoglu, *Phys. Rev. Lett.* **109**, 107401 (2012).
 [34] C. Santori, S. Götzinger, Y. Yamamoto, S. Kako, K. Hoshino, and Y. Arakawa, *Appl. Phys. Lett.* **87**, 051916 (2005).
 [35] M. F. Doty, M. Scheibner, I. V. Ponomarev, E. A. Stinaff, A. S. Bracker, V. L. Korenev, T. L. Reinecke, and D. Gammon, *Phys. Rev. Lett.* **97**, 197202 (2006).
 [36] M. L. Andersen, S. Stobbe, A. S. Sørensen, and P. Lodahl, *Nat. Phys.* **7**, 215 (2010).
 [37] C. F. Wang, A. Badolato, I. Wilson-Rae, P. M. Petroff, E. Hu, J. Urayama, and A. Imamoglu, *Appl. Phys. Lett.* **85**, 3423 (2004).
 [38] R. Lettow, Y. L. A. Rezus, A. Renn, G. Zumofen, E. Ikonen, S. Götzinger, and V. Sandoghdar, *Phys. Rev. Lett.* **104**, 123605 (2010).
 [39] Z. Nie, A. Petukhova, and E. Kumacheva, *Nat. Nanotechnol.* **5**, 15 (2009).

- [40] Z. Gueroui and A. Libchaber, *Phys. Rev. Lett.* **93**, 166108 (2004).
- [41] R. Schreiber, J. Do, E. M. Roller, T. Zhang, V. J. Schüller, P. C. Nickels, J. Feldmann, and T. Liedl, *Nat. Nanotechnol.* **9**, 74 (2013).
- [42] J. D. Cox, M. R. Singh, C. von Bilderling, and A. V. Bragas, *Adv. Opt. Mater.* **1**, 460 (2013).
- [43] L. Zhang, J. Lou, and L. Tong, *Photon. Sensors* **1**, 31 (2010).
- [44] K. P. Nayak, P. N. Melentiev, M. Morinaga, F. Le Kien, V. I. Balykin, and K. Hakuta, *Opt. Express* **15**, 5431 (2007).
- [45] J. D. Cox, M. R. Singh, G. Gumbs, M. A. Antón, and F. Carreño, *Phys. Rev. B* **86**, 125452 (2012).
- [46] K. Bergmann, H. Theuer, and B. W. Shore, *Rev. Mod. Phys.* **70**, 1003 (1998).
- [47] M. A. Antón, F. Carreño, S. Melle, O. G. Calderón, E. Cabrera-Granado, J. D. Cox, and M. R. Singh, *Phys. Rev. B* **86**, 155305 (2012).